



ELSEVIER

Contents lists available at SciVerse ScienceDirect

Earth and Planetary Science Letters

journal homepage: www.elsevier.com/locate/epsl

Characterizing and quantifying iron oxides in Chinese loess/paleosols: Implications for pedogenesis



Pengxiang Hu^a, Qingsong Liu^{a,*}, José Torrent^b, Vidal Barrón^b, Chunsheng Jin^c

^a State Key Laboratory of Lithospheric Evolution, Institute of Geology and Geophysics, Chinese Academy of Sciences, Beijing 100029, China

^b Departamento de Agronomía, Universidad de Córdoba, Edificio C4, Campus de Rabanales, 14071 Córdoba, Spain

^c Division of Cenozoic Geology and Environment, Institute of Geology and Geophysics, Chinese Academy of Sciences, Beijing 100029, China

ARTICLE INFO

Article history:

Received 25 April 2012

Received in revised form

19 March 2013

Accepted 23 March 2013

Editor: G. Henderson

Available online 16 April 2013

Keywords:

pedogenesis

magnetic iron oxides

dissolution

rock magnetism

diffuse reflectance spectroscopy

Chinese loess

ABSTRACT

To accurately decode the paleoclimatic and paleoenvironmental significance of magnetic properties in Chinese loess/paleosols, neof ormation of magnetic iron oxides via pedogenesis as well as the relationship between ferrimagnetic (maghemite and magnetite) and antiferromagnetic minerals (hematite and goethite) of both detrital and pedogenic origins should be well determined. To resolve this problem, magnetic iron oxides from a contiguous loess–paleosol sequence (lower part of the loess unit L1, paleosol unit S1, and the upper part of L2) at Luochuan, Center of the Chinese Loess Plateau, were well characterized and quantified by using an integrated approach including chemical dissolution, diffuse reflectance spectroscopy and rock magnetism methods. Results showed that these magnetic minerals have distinct coercivity and dissolution behavior, which is highly grain size-dependent. More specifically, the paleosol is enriched with nano-sized pedogenic hematites with a medium coercivity of ~130 mT, which are also preferentially dissolved in a weak reductive environment. In contrast, the coarse-grained micro-sized detrital hematites with a medium coercivity of ~1 T are dominant in loess. In addition, these coarse-grained detrital hematites are more stoichiometric than their pedogenic counterparts as evidenced by the higher band position on the diffuse reflectance spectrum. Goethite can be well distinguished from hematite by its higher coercivity (4–7 T) at low temperature (10 K). The consistent dissolution behavior of goethite for both loess and paleosol samples in citrate–bicarbonate–dithionite solution indicates that goethite could be less relevant to the pedogenic processes. The reductive dissolution of pedogenic maghemite lags the dissolution of pedogenic hematite and fine-grained goethite, which suggests that average grain size of pedogenic maghemite is relatively larger than those of pedogenic hematite and fine-grained goethite. Detrital magnetite is hard to dissolve and ~50% of its initial remanence survived after dissolution. On the basis of these contrasting behaviors, pedogenic hematite, fine grained goethite and maghemite content was further quantified. Our results suggest that single domain pedogenic hematite was produced after initial formation of pedogenic maghemite. This provides direct evidence for the recently proposed pathway in which ferrihydrite is transformed into a transient maghemite-like phase before its final transformation into hematite.

© 2013 Elsevier B.V. All rights reserved.

1. Introduction

Soil magnetic enhancement is one of the most fascinating phenomena in both geological and environmental research (Boyle et al., 2010; Dearing et al., 1996; Evans and Heller, 1994; Le Borgne, 1955; Maher, 1998; Mullins, 1977; Quinton et al., 2011; Singer et al., 1996; Torrent et al., 2006; Zhou et al., 1990). Typically, the periodical rhythm of magnetic enhancement recorded by the Chinese loess/paleosols sequence reflects paleoclimate changes at different time scales, and can be further linked to the marine

oxygen isotope records (Bloemendal et al., 1995; Heller and Liu, 1986; Kukla et al., 1988).

However, how magnetic iron oxides respond to pedogenesis is still a matter of debate. So far, several mechanisms have been proposed to interpret magnetic enhancement for (paleo) soils, such as the biotic (Fassbinder et al., 1990; Lovley et al., 1987) or fermentation mechanism (Le Borgne, 1955; Mullins, 1977). Later, studies showed that neof ormation of pedogenic ferrimagnetic minerals are mainly controlled by a series of abiotic reactions (Dearing et al., 1996; Maher and Taylor, 1988; Torrent et al., 2006). More recently, Boyle et al. (2010) established a chemical kinetic model which further confirmed that abiotic reactions should account for most production of ferrimagnetic minerals. However, the exact pathway has not been fully articulated.

On the one side, the ferrihydrite → maghemite-like phase → hematite pathway was proposed by Barrón and Torrent (2002),

* Correspondence to: Institute of Geology and Geophysics, Chinese Academy of Sciences, No. 19, Beitucheng Western Road, Chaoyang District, 100029 Beijing, China. Tel.: +86 10 82998365; fax: +86 10 62010846.

E-mail address: liux0272@yahoo.com (Q. Liu).

Barrón et al. (2003), Torrent et al. (2006) and Cabello et al. (2009) on the basis of experiments in which ferrihydrite doped with some ligands (e.g. phosphate or citrate) was aged at different temperatures. Recently, Michel et al. (2010) revealed that this maghemite-like phase is ordered ferrihydrite with strong magnetism, which can be further evolved into maghemite with grain growing from superparamagnetic (SP) to single domain (SD) size before their transformation (Barrón et al., 2012; Liu et al., 2008a; Michel et al., 2010). This model was also supported by the linear relationship between the concentration of hematite and pedogenic maghemite (Liu et al., 2010b; Torrent et al., 2006, 2007, 2010).

On the other hand, Dearing et al. (1996) suggested the ferrihydrite → magnetite → maghemite pathway and Maher (1998) also preferred that maghemite was not formed directly, but through the oxidation of magnetite. By integrating different conceptual models with existing experimental and field data, Boyle et al. (2010) suggested a comprehensive mechanism which hydrous ferric oxide could either transform directly to hematite and goethite or magnetite which later oxidized to maghemite.

To provide further evidence on the pedogenic processes leading to magnetic iron oxides, it is crucial to systematically investigate the major magnetic components of pedogenic origin and their relationships during pedogenesis. This requires pedogenic components to be separated from detrital inputs either by physical or chemical methods. For physical separation, an efficient approach is the particle size separation using a combination of sieving and pipetting (Hao et al., 2008; Zheng et al., 1991). Consistent relationships between particle size and magnetic properties were found in sediments from diverse environments including Chinese loess (Oldfield et al., 2009; Oldfield and Yu, 1994), which facilitates the identification of sediments from different processes or sources (Hao et al., 2008; Sartori et al., 2005).

Ferrimagnetic minerals of detrital and pedogenic origins have also been successfully discriminated via extraction with the citrate–bicarbonate–dithionite (CBD) reagent, which results in dissolution of pedogenic magnetite and maghemite leaving coarse magnetite in the residue (Fine et al., 1995; Hunt et al., 1995; Singer et al., 1995). In addition, decomposition of the isothermal remanent magnetization

(IRM) acquisition curve can also be used to study the different magnetic components of a mixture on the basis of their different mean coercivity spectra (Egli, 2004; Heslop et al., 2002; Kruiver et al., 2001; Robertson and France, 1994; Spassov et al., 2003).

Regardless of these previous studies, the accurate relationship between weakly antiferromagnetic minerals (hematite and goethite, the final products of pedogenesis in aerobic environment) with strongly magnetic minerals (magnetite and maghemite) has not been well established.

To accurately quantify the relationship between ferrimagnetic and antiferromagnetic minerals in Chinese loess, and to cast strong constraints on pedogenic process, this paper utilizes a comprehensive approach by integrating IRM decomposition analysis, dynamic CBD dissolution (Torrent et al., 2010), low temperature IRM technology (Bógalo et al., 2001), and diffuse reflectance spectroscopy (DRS) (Deaton and Balsam, 1991; Ji et al., 2002; Liu et al., 2011; Torrent and Barrón, 2003). Finally, detailed pedogenic pathways will be addressed based on the systematic analysis of the relationships between the different iron oxides.

2. Sampling and methods

2.1. Sampling

A loess–paleosol–loess transition sequence from the classic Luochuan section in the central part of Chinese Loess Plateau (CLP) was collected (Fig. 1). Samples comprise of the loess (L) and paleosol (S) units of L1–S1–L2 (Liu and Ding, 1998). Together, 30 samples were selected at 7.5 cm intervals around the loess–paleosol boundary and 17.5 cm intervals in the central part of S1 paleosol.

2.2. Magnetic methods

Magnetic susceptibility (mass-specific) was measured using the AGICO MFK1-FA Multi-function Kappabridge control unit at dual frequencies of 976 Hz (low frequency) and 15,616 Hz (high

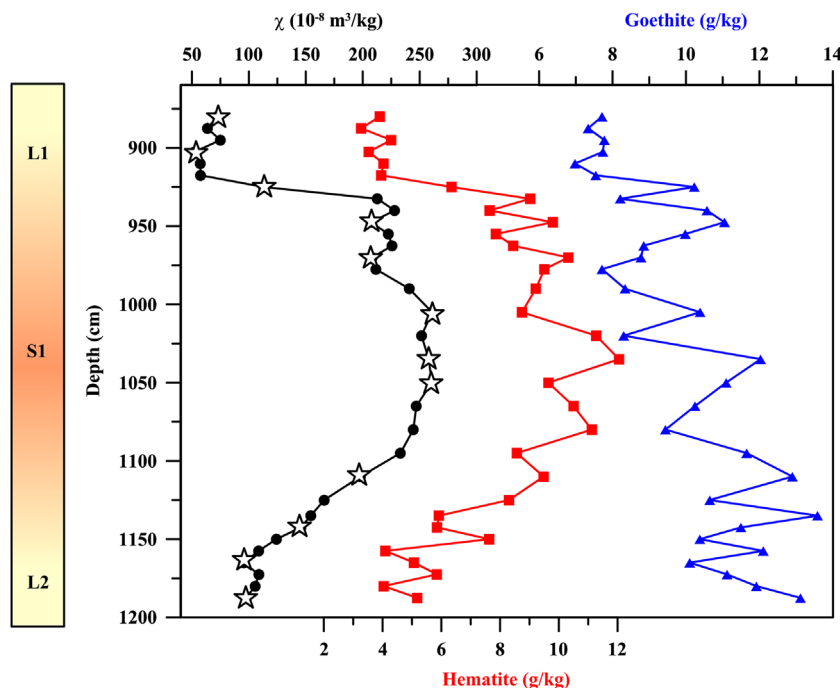


Fig. 1. Schematic representation of the sampled section. The depth variation of low field susceptibility, χ (circles); concentration of hematite (squares); concentration of goethite (triangles) were shown. Stars represent the 12 samples selected for chemical dissolution.

frequency). The sensitivity is $\sim 10^{-11} \text{ m}^3 \text{ kg}^{-1}$ and the accuracy is 0.1% (Hrouda, 2011). The corresponding values are referred to χ_L and χ_H , respectively. The frequency-dependent susceptibility was defined as $\chi_{FD} = (\chi_L - \chi_H)$, which is proportional to the concentration of the viscous SP particles (Worm, 1998). Without further explanation, in the following sections, χ refers to χ_L .

Because the pedogenic maghemite in Chinese loess/paleosols has a rather broad grain size distribution (Liu et al., 2005), Xu et al. (2012) confirmed that for Chinese loess samples, χ and χ_{FD} measured at different frequencies all display linear relationship. Hrouda (2011) further showed that χ_{FD} (976–15,616 Hz) measured by MFK1-FA has the highest value and is thus more suitable for weakly magnetic samples.

Anhysteretic remanent magnetization (ARM) was imparted in an alternating field of 100 mT with a superimposed 50 μT bias field, and was then expressed by ARM susceptibility (χ_{ARM}). Saturation magnetization (M_s), saturation remanent magnetization (M_{rs}), coercivity (B_c) and remanent coercivity (B_{cr}) were measured using a Princeton Measurements Corporation vibrating sample magnetometer (Micromag VSM 3900) after correcting for the paramagnetic contribution.

High field IRM acquisition curves (up to 5 T) at 300 K and 10 K of selected samples were obtained by Quantum Designs Magnetic Property Measurement System (MPMS) in 32 steps from 6 mT to 5 T. These IRM acquisition curves were then decomposed to sets of log-Gaussian curves (Kruiver et al., 2001). Only gradient acquisition plots (GAP) are shown in Fig. 5. Detailed Gaussian function parameters—distribution width (DP) at half peak intensity, mean coercivity at half distribution width ($B_{1/2}$) are summarized in Tables 1 and 2.

Table 1

Values of SIRM ($10^{-5} \text{ Am}^2/\text{kg}$), midpoint $B_{1/2}$ (mT) and dispersion (DP) of the IRM components in loess and paleosol samples at 300 K. The DP is given in log-field values. 0.1 g represents sample treated by 0.1 g dithionite.

300 K	Comp. 1			Comp. 2			Comp. 3		
	SIRM	$B_{1/2}$	DP	SIRM	$B_{1/2}$	DP	SIRM	$B_{1/2}$	DP
Loess									
Original	641	50	0.48	30	126	0.20	43	1734	0.30
0.1 g	650	54	0.45	17	126	0.12	43	2188	0.30
0.2 g	464	68	0.39				35	1730	0.35
1.2 g	343	67	0.40				9	1585	0.40
Paleosol									
Original	1360	26	0.35	200	127	0.20	104	1000	0.27
0.1 g	1360	28	0.40	100	159	0.20	100	794	0.30
0.2 g	774	44	0.47	38	159	0.20	51	1349	0.30
1.2 g	373	59	0.40				15	1778	0.30

Table 2

Values of SIRM ($10^{-5} \text{ Am}^2/\text{kg}$), midpoint $B_{1/2}$ (mT) and dispersion (DP) of the IRM components in loess and paleosol samples at 10 K. The DP is given in log-field values. 0.1 g represents sample treated by 0.1 g dithionite.

10 K	Comp. 1			Comp. 2			Comp. 3			Comp. 4		
	SIRM	$B_{1/2}$	DP									
Loess												
Original	1320	76	0.32	150	224	0.20	450	1005	0.47	470	5754	0.25
0.1 g	1250	71	0.32	135	224	0.18	350	1000	0.38	350	5623	0.21
0.2 g	835	106	0.37				176	1259	0.38	180	6918	0.15
1.2 g	633	122	0.35				123	1585	0.40	180	6607	0.10
Paleosol												
Original	3600	60	0.25	804	200	0.20	764	794	0.25	700	3981	0.27
0.1 g	3360	56	0.25	600	200	0.20	600	794	0.25	600	5888	0.25
0.2 g	1270	59	0.30	279	200	0.20	330	794	0.30	200	5888	0.22
1.2 g	800	100	0.35				190	794	0.29	200	6310	0.20

Low temperature dependence χ - T curves were also measured at two frequencies (1 Hz and 1000 Hz) from 10 K to 300 K using MPMS. For the low temperature measurements, χ_{FD} is defined as $\chi_{1 \text{ Hz}} - \chi_{1000 \text{ Hz}}$. The applied field was set to be 0.4 mT.

2.3. Non-magnetic methods

The reductive dissolution curves of 12 representative samples (Fig. 2) were obtained using the CBD reagent (Mehra and Jackson, 1960) at 50 °C. For each sample, dithionite (the reductant) rates ranging from 0 to 1.2 g (0, 0.04, 0.08, 0.1, 0.12, 0.14, 0.16, 0.2, 0.4, 1.2 g) per 50 ml was used on 10 parallel samples in order to achieve an increasing degree of reductive dissolution (little iron was further extracted when more than 1.2 g dithionite was used). The total iron in solution was determined colorimetrically with the o-phenanthroline method (Olson and Ellis, 1982), using a measuring wavelength of 508 nm. The residual was washed twice with 0.01 M CaCl₂, twice with deionized water and dried at 36 °C for further DRS and magnetic measurements.

The DR spectra were recorded by a Cary 5000 UV-vis-IR spectrophotometer (Varian Inc., Palo Alto, CA) equipped with an integrating sphere accommodating a PMT/PbS detector at a scan rate of 30 nm/min from 300 to 2600 nm in 0.5 nm steps. Then the reflectance values were transformed into the Kubelka-Munk (K-M) remission function and the bands of the second derivative of the K-M function spectrum were used to quantitatively estimate the relative mass concentration of hematite and goethite, as described in detail by Torrent et al. (2007). The absolute concentration of hematite and goethite were calculated by assigning all CBD extractable iron (Fe_d) to these two minerals. The contribution of ferrihydrite and magnetite/maghemite was ignored, because their contribution to Fe_d is rather limited (Torrent et al., 2007).

In this study, total iron in hematite and goethite for each selected loess or paleosol sample was defined as $\text{Fe}_{d-1.2 \text{ g}}$, which was extracted using 1.2 g dithionite. Therefore, the Fe_d used to calculate the concentration of hematite and goethite in each parallel sample is $\text{Fe}_{d-1.2} - \text{Fe}_{d-x}$, where x represents the amount of dithionite added to 50 mL of the citrate-bicarbonate extracting solution.

3. Results

3.1. Dynamic reductive dissolution of iron oxides

3.1.1. Concentration variations

The loss of magnetic iron oxides during dynamic dissolution is illustrated in Fig. 2. Overall, the concentration of each magnetic iron oxide decreases with iron dissolution but in different ways.

Goethite is steadily dissolved with comparable trends in both loess and paleosol samples (Fig. 2a), indicating the similar dissolution behavior of loess and paleosol goethite. In contrast, hematite exhibits distinct dissolution patterns in loess and paleosol samples (Fig. 2b), which reveal two types of hematites: (1) easily-dissolved hematite, which is enriched in the paleosol samples; (2) hard-dissolved hematite that exists both in loess and paleosol samples.

M_s mainly represents the concentration of magnetite and maghemite. It remains constant initially and then starts to decrease (Fig. 2c), which indicates that ferrimagnetic minerals are more resistant to dissolution than the easily-dissolved hematite and goethite. After full CBD dissolution, more than 20% of M_s remains while hematite and goethite are hardly detected (Fig. 2a–c).

χ_{FD} is stable at the beginning of dissolution but then quickly decreases (Fig. 2d). The different behavior of M_s and χ_{FD} basically indicates that ultrafine pedogenic magnetite and maghemite particles are mostly dissolved, leaving coarser-grained magnetic particles in the residue which are responsible for the remaining M_s .

Based on Fig. 2, two dissolution steps are defined to illustrate the dissolution behavior of magnetic iron oxides: Step I, less than 20% hematite was dissolved in the least-weathered loess samples (880 cm, 902.5 cm and 1187.5 cm), less than 20% χ_{FD} and M_s was reduced in most samples but up to 40% hematite is lost in the paleosol samples (red symbols); Step II, all magnetic iron oxides show linear dissolution trend for both loess and paleosol samples.

3.1.2. Grain size change

The dissolution processes also results in grain size change. At the initial stage, hysteresis parameters uniformly plot toward the SD region on a Day plot (Day et al., 1977; Dunlop, 2002a, 2002b) (Fig. 3a and c). The ratio χ_{ARM}/χ , which is highly sensitive to the stable SD particles (Banerjee et al., 1981; King et al., 1982) and commonly used as a grain size proxy, displays an increasing trend (Fig. 3b and d). All these variation indicate an enhanced proportion of SD particles. Then, as more iron is dissolved, points on Day plot move in the opposite direction toward coarser MD region (Fig. 3a and c) and accompanied by rapidly declination of χ_{ARM}/χ , which represents a significant coarsening.

The effects of the dissolution process on SP particles can be more clearly traced by the $\chi_{FD}-T$ curves (Fig. 4). For nano-sized particles, the peak and the absolute value of $\chi_{FD}-T$ curve are directly related to the average grain size and concentration of these fine grains (Liu et al., 2005). With increasing degree of reduction, the absolute χ_{FD} values gradually decrease (Fig. 4a), indicating the depletion of SP particles. At the same time, the temperature of maximum χ_{FD} systematically increases (Fig. 4b), which represents that the mean particle volume becomes larger. In addition, the dissolved particles exhibit a peak value at ~ 150 K (Fig. 4c and d), which corresponds to grain size < 20 nm for maghemite (Liu et al., 2004b). This evidence strongly demonstrates that finer SP particles are dissolved in preference to the coarser SD

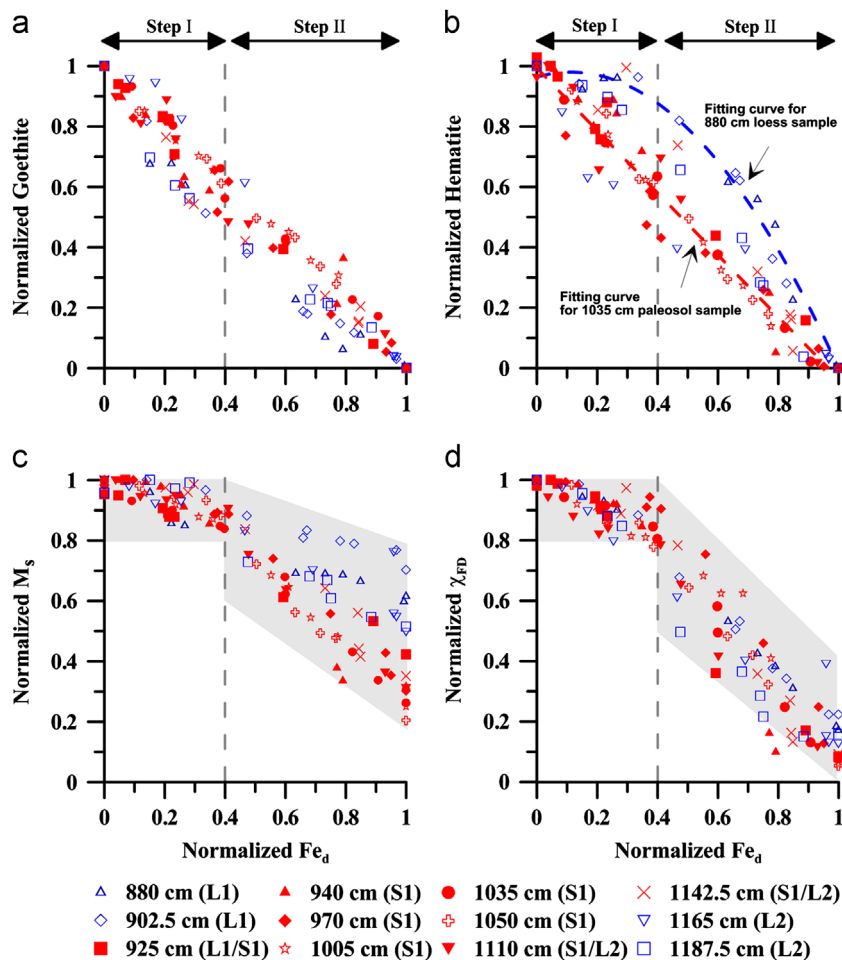


Fig. 2. Dissolved iron, Fe_d , as a function of concentration of goethite (a); concentration of hematite (b) (for clarity, only two fitting curves for representative loess and paleosol sample were shown to display the dissolution trend); M_s (c); and χ_{FD} (d) during CBD dissolution. All values are normalized to the maximum. Shaded areas on (c) and (d) represent the general dissolution trend. The Roman numerals indicate the dissolution steps defined in the text. (For interpretation of the references to color in this figure, the reader is referred to the web version of this article.)

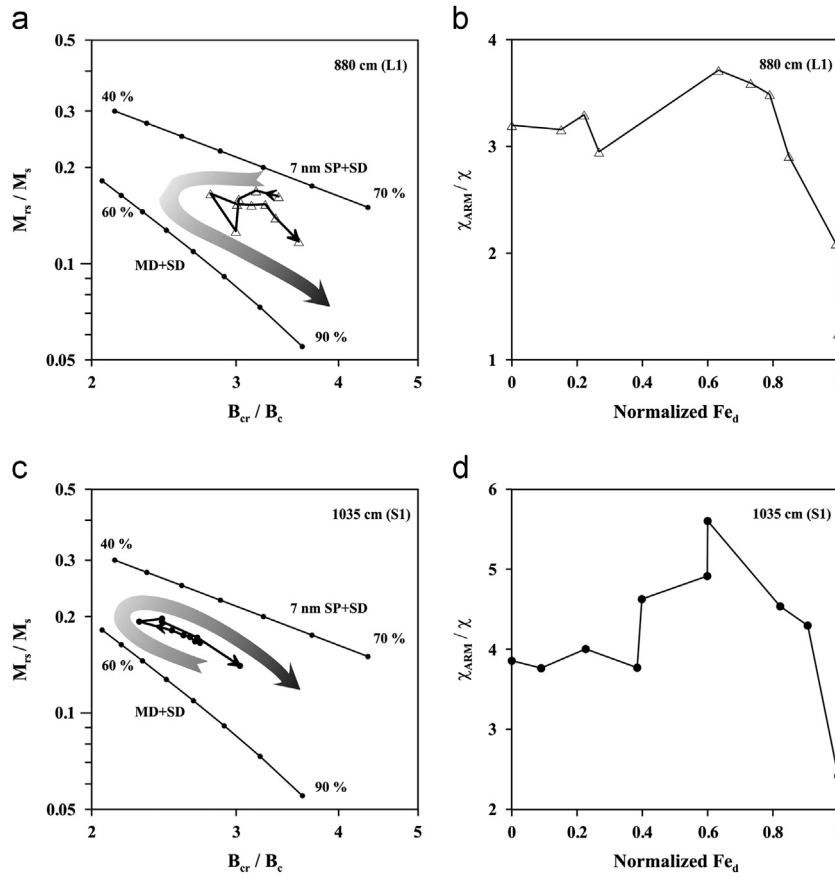


Fig. 3. Day plots of representative loess (a) and paleosol (c) sample during dissolution process. The thick gradient arrows represent the general trend of each data series. The change of χ_{ARM}/χ ratio during dissolution was also shown in (b) and (d) for loess and paleosol, respectively. The interpretation framework is after Dunlop (2002a).

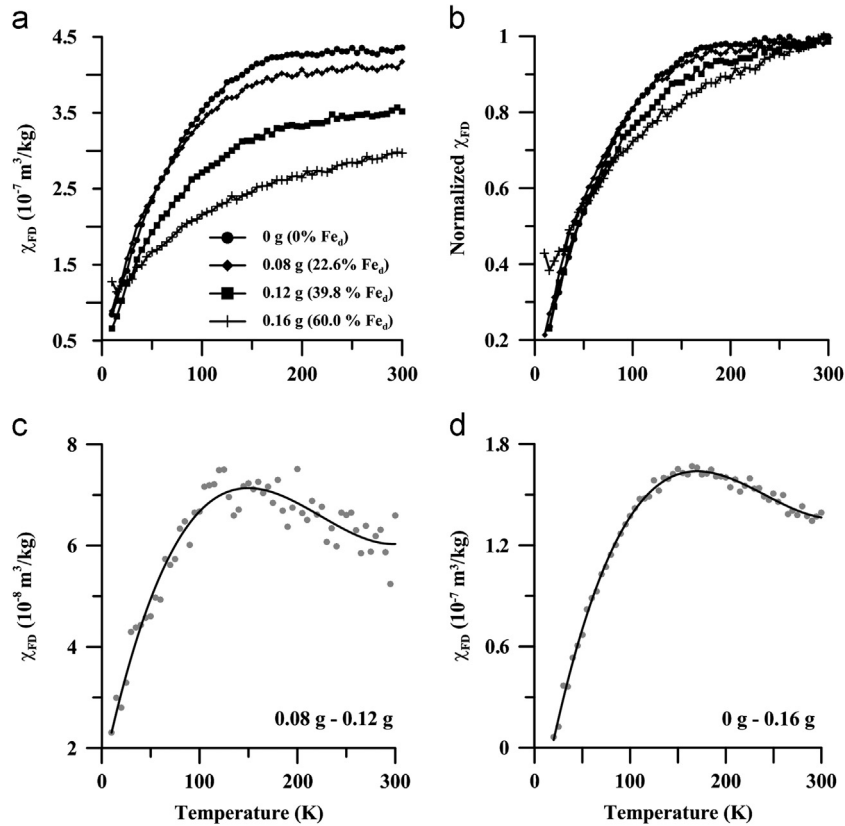


Fig. 4. $\chi_{FD}-T$ curves of a typical paleosol sample using four amounts of dithionite for 10–300 K range. (a) the raw data; (b) normalized χ_{FD} ; (c) the difference in χ_{FD} between the subsample treated with 0.08 g and that treated with 0.12 g of dithionite; (d) the difference of χ_{FD} between the subsample untreated dithionite and that treated with 0.16 g of dithionite (grey solid circles: raw data; black solid line: 3rd polynomial fitting curves). The corresponding Fe_d for each subsample is also given.

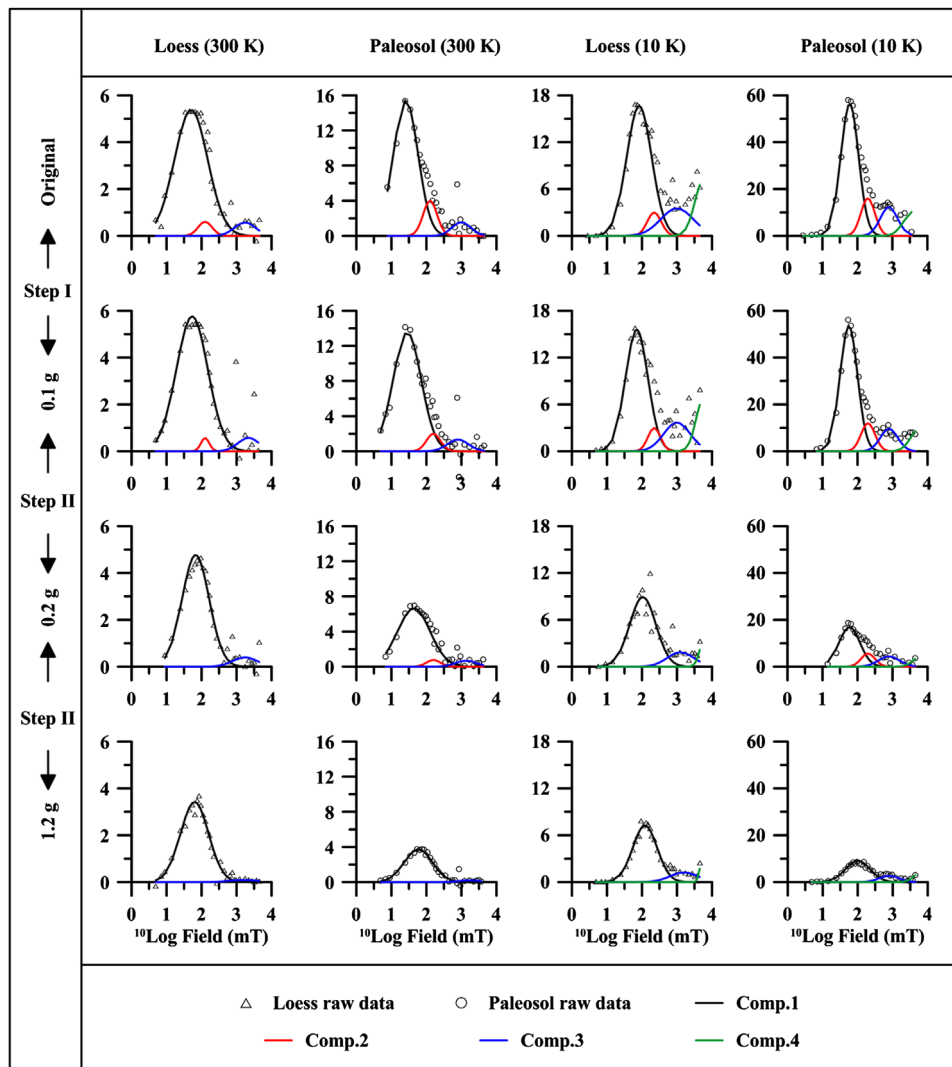


Fig. 5. Examples of IRM component analyses: GAP for typical loess and paleosol samples treated with different amounts of dithionite (0, 0.1, 0.2, 1.2 g). (open triangles: loess raw data; open circles: paleosol raw data; black line: Comp. 1; red line: Comp. 2; blue line: Comp. 3 and green line: Comp. 4). (For interpretation of the references to color in this figure legend, the reader is referred to the web version of this article.)

ones. Thus, the initial trend towards SD region on Day plot and the increase in χ_{ARM}/χ indicates the loss of SP particles. However, only $\sim 20\%$ χ_{FD} is lost in Step I, suggesting even fine SP particles are mainly removed in Step II. Overall, combining the results of Day plot and $\chi_{FD}-T$ curves, the reductive dissolution of magnetite and maghemite reflects a gradual coarsening throughout the whole process.

3.2. IRM component analyses

The IRM component analyses identify three components in both loess and paleosol samples at 300 K (Fig. 5): (1) a low-coercivity component (< 50 mT) (Comp. 1); (2) a medium-coercivity component (Comp. 2) with $B_{1/2}$ of ~ 130 mT, and DP ranging between 0.15 and 0.20; and (3) a high-coercivity component with $B_{1/2}$ between 1 and 1.7 T (Comp. 3). Detailed variations for $B_{1/2}$ and IRM at different degrees of dissolution are summarized in Table 1 and illustrated on Fig. 6.

Comp. 1 is the major IRM carrier in both loess and paleosol. Upon dissolution, it remains stable at Step I, but decreases significantly in Step II (Fig. 6a and c). However, a significant portion of IRM contributed by Comp. 1 remains after dissolution, especially for loess sample. Its mean coercivity also becomes higher but uniform

in loess and paleosol samples (Fig. 6b and d; Table 1). Comp. 3 is also identified in all samples, and dissolved mostly during the Step II (Fig. 6a and c). Unlike the above two components, Comp. 2 is enhanced in paleosols, with narrower distribution of coercivity, and about 50% of its IRM is removed at the initial dissolution step (Fig. 6a and c).

At 10 K, all these three components shift to higher mean coercivity and greatly increase in intensity (Fig. 5, Table 2). This is possibly due to the blocking behavior of SP particles and their increasing ability of getting residual magnetism with decreasing temperature (Dunlop and Özdemir, 1997). Remarkably, a non-saturated Comp. 4 with an extremely large coercivity (4–7 T) appears in both loess and paleosol, characterized by gradual decrease of IRM intensity and increase of $B_{1/2}$ upon dissolution (Fig. 6a, c and Table 2).

4. Discussion

4.1. Characterization of magnetic iron oxides

Characterization of magnetic iron oxides of detrital and pedogenic origin is the prerequisite to clarify their relationship in soil

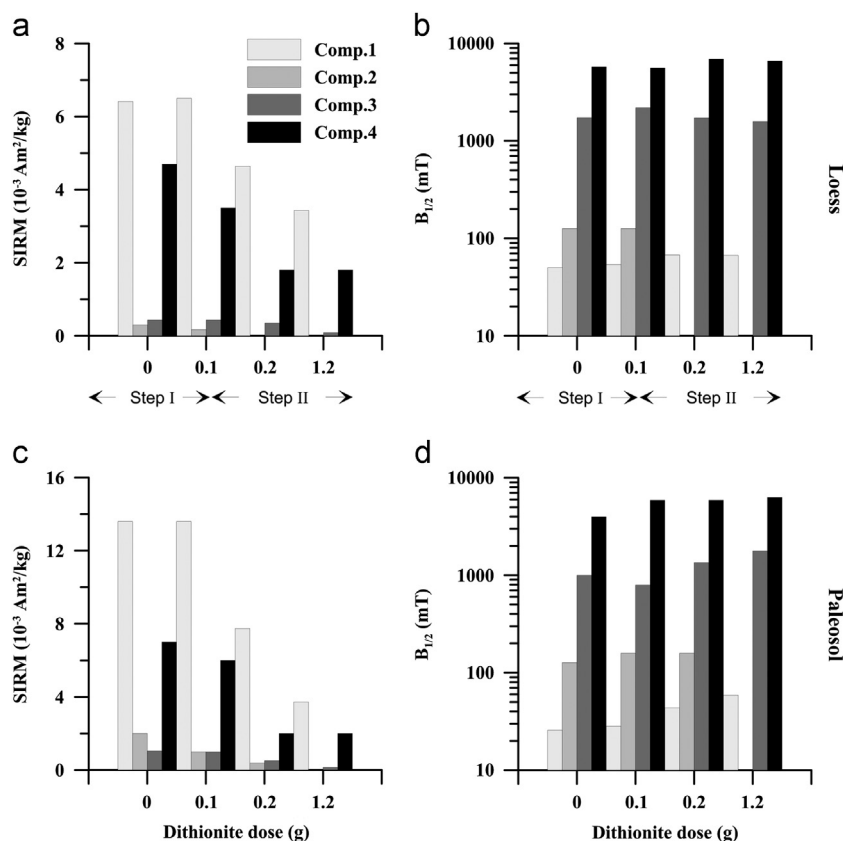


Fig. 6. Variation of SIRM ($10^{-3} \text{ Am}^2/\text{kg}$) and midpoint coercivity $B_{1/2}$ (mT) for four components identified in loess (a and b) and paleosol (c and d) samples upon CBD dissolution. The values for Comp. 1, Comp. 2 and Comp. 3 are obtained at 300 K, values for Comp. 4 is obtained at 10 K.

forming process and further provide constrains on their pedogenic pathways. In this study, multiple interdisciplinary methods enable us the dynamic separation and more delicate description of the different magnetic components in Chinese loess and paleosol.

IRM decomposition reveals four components based on their coercivity spectrum (Fig. 5); among them, Comp. 4 is the most distinctive one. It is only clearly detected at low temperature with an extremely large coercivity ($B_{1/2}$ of 4–7 T, Table 2 and Fig. 6b and d). Moreover, it cannot be saturated even at 5 T (Fig. 5). All these intrinsic properties lead to goethite, which is the most common antiferromagnetic iron oxide in soils and possesses an additional weak parasitic but hard ferromagnetism below its Néel Temperature (T_N) (Banerjee, 1970; Dekkers, 1989; Özdemir and Dunlop, 1996). Although both hematite and goethite show much higher coercivity than ferrimagnetic minerals, goethite has high exchange energies of the magnetic sublattices and extremely weak M_s , resulting in coercive forces up to hundreds of mT (Dunlop and Özdemir, 1997). Also due to its low M_s , large fields are needed to deflect the magnetic moments. As a result, significant remanence acquisition of goethite begins at least above 1 T and sometimes no saturation of IRM occurs even at 20 T (Dekkers, 1989; France and Oldfield, 2000; Maher et al., 2004; Rochette et al., 2005). The Néel temperature for pure goethite is about 395–400 K (Özdemir and Dunlop, 1996), but most natural samples consist of small crystals and exhibit Al-for-Fe substitution (Cornell and Schwertmann, 2003, and references therein), which suppresses T_N below the room temperature through reducing AB (the two sublattices in the goethite structure) interaction by increasing Al contents and crystal defects (Liu et al., 2004c). Therefore, goethite is usually not detected in room temperature magnetic analyses as it becomes paramagnetic. However, upon cooling, not only goethite changes from paramagnetic into weak ferromagnetic but also the remanence of goethite is

significantly enhanced (Dekkers, 1989; Liu et al., 2006; Maher et al., 2004). That is why goethite was only identified at 10 K. Moreover, the IRM intensity of Comp. 4 gradually reduced through Step I and Step II, also fitting the dissolution behavior of goethite in Fig. 2a.

Comp. 1 was also well identified because it accounted for ~90% of total IRM (Fig. 6a and c). Another significant trait is that it generally saturated below 100 mT (Fig. 5). These two properties suggest a strong and “soft” ferrimagnetic nature (Dunlop and Özdemir, 1997; Verosub and Roberts, 1995). However, Comp. 1 in loess and paleosol had distinct average coercivity (~50 and ~25 mT, respectively) and coercivity distribution (0.48 and 0.35, respectively), suggesting different origins.

The ferrimagnetic assemblage in Chinese loess/paleosols consists of both detrital and pedogenic components (Evans and Heller, 1994; Liu et al., 2007; Spassov et al., 2003). Eolian coarse-grained magnetite with different degree of oxidation and low-Ti titanomagnetite makes up the major detrital components while the pedogenic phase consists mainly of fine-grained ferrimagnetic minerals (Fine et al., 1993; Liu et al., 2003, 2007; Spassov et al., 2003; Zhou et al., 1990).

Detrital components originate from dust accumulation and are generally considered as the carriers of magnetic “background” in loess/paleosols sequences. The grain size of detrital particles can reach several to tens of micrometers according to SEM results (Chen et al., 2010). A significant magnetic feature of detrital magnetite/titanomagnetite is their higher coercivity and wider distribution (Egli, 2004; Spassov et al., 2003). Theoretically, for SD magnetite, coercivity increased with increasing grain size and reached the maximum at the boundary of SD and PSD; then, it dramatically decreased (Dunlop and Özdemir, 1997; Maher, 1988). However, in nature, eolian PSD/MD grained magnetite/titanomagnetite also has much higher coercivity due to its high internal

stress caused by the mismatch of unit cell between the oxidized maghemite rim and the magnetic core (Liu et al., 2003; van Velzen and Dekkers, 1999). Spassov et al. (2003) decomposed IRM acquisition of similar loess and paleosol samples of the CLP and identified detrital magnetite and maghemite with coercivity values of ~ 79 and 113 mT, respectively. In this study, Comp. 1 peaks at $B_{1/2}$ value of ~ 50 mT in loess with a wide distribution (0.35–0.45), which fits well with the characteristic coercivity value obtained from unweathered SD and PSD magnetite, both synthetic and in loess/paleosols (Dunlop and Özdemir, 1997; Maher, 1988; Spassov et al., 2003; van Oorschot et al., 2002). More importantly, after CBD dissolution, despite the original differences of Comp. 1 between loess and paleosol, uniform $B_{1/2}$ and DP values were achieved which were similar to those of the original loess (Figs. 5, 6b, d and Table 1). Since the CBD method is well known for its efficiency in removing pedogenic iron oxides (Fine et al., 1995; Hunt et al., 1995; Singer et al., 1995), this dissolution behavior again signaled detrital magnetite as the major carrier of Comp. 1 in loess.

By contrast, Comp. 1 obtained in the paleosol exhibited reduced $B_{1/2}$ (~ 25 mT) and distribution value (0.35) but greatly increased intensity (Fig. 6c, d and Table 1). This behavior is consistent with the magnetic properties of pedogenic ferrimagnetic minerals, which are responsible for magnetic enhancement in paleosols (Zhou et al., 1990; Liu et al., 2004a). The grain size distribution of pedogenic magnetic particles is fairly uniform with maximum concentration just above the SP/SD threshold (Liu et al., 2004b, 2005). Therefore, under the influence of strong thermal agitation, pedogenic components have relatively lower coercivity (Evans and Heller, 2001; Fukuma and Torii, 1998). Previous IRM decomposition work also showed the midpoint coercivity for pedogenic maghemite/magnetite to be only ~ 30 mT (Eyre, 1996; Spassov et al., 2003; van Oorschot et al., 2002). Other coercivity reports obtained by different methods also gave comparable values (Egli, 2004; Evans and Heller, 2001; Geiss and Zanner, 2006). Evidences also come from the dissolution behavior, in which small SP/SD particles were removed according to the low temperature χ - T curves and Day plots (Figs. 3 and 4). Based on the simulation of Liu et al. (2005), the removed particles correspond to maghemite around 20 nm, right at the boundary of SP/SD. Therefore, Comp. 1 of paleosol shifted to the coercivity of loess after dissolution because only large detrital particles were left (Figs. 5, 6b and d). Whether magnetite or maghemite is the dominant product of pedogenesis remains controversial, but given that magnetite can be easily oxidized into maghemite because of its high surface to volume ratio (Chen et al., 2005; Cornell and Schwertmann, 2003; van Velzen and Dekkers, 1999), we assign pedogenic maghemite as the major carrier of Comp. 1 in paleosol.

Comp. 2 is both observed in the IRM decomposition spectra of loess and paleosol with a peak coercivity of ~ 130 mT (Fig. 6b and d). Components with similar coercivity have been reported in other CLP loess/paleosol sections (Eyre, 1996; Spassov et al., 2003), where it was interpreted as detrital maghemite or titanomagnetite because it contributed more in loess than paleosol. However, Comp. 2 displays a remarkable pedogenic character not only because IRM intensity is enhanced almost seven times in the paleosol (Fig. 6a and c), but also because of the narrow coercivity distribution (DP: 0.1–0.2) (Table 1). Pedogenic antiferromagnetic mineral such as hematite is also formed in soil forming process, which caused the reddish color of paleosols (Chen et al., 2002). Observation of pedogenic hematite from CLP shows they are several to about one hundred nanometers in grain size (Chen et al., 2010). According to numerous reports on the SP and SD boundary of hematite, pedogenic hematite in Chinese loess lies just around the boundary of SP/SD (Banerjee, 1971; Dunlop, 1971; Kletetschka and Wasilewski, 2002 and references therein). For SD

particles, the coercivity of hematite increases with grain size until it reaches the maximum at the SD threshold (Dekkers and Linssen, 1989). As hematite approaches SD/SP boundary, coercivity decreases. For example, Rath et al. (1999) reported the coercivity of trapezoidal hematite with particle size of 40–80 nm to be only 43.5–61.5 mT. Therefore, 130 mT is a reasonable coercivity value for pedogenic fine-grained hematite. Moreover, according to Figs. 5 and 6c, Comp. 2 is significantly removed at the initial stage of dissolution, consistent with the initial fast dissolution of hematite (Fig. 2b) and the IRM intensity of Comp. 2 is linearly correlated with χ_{FD} (Fig. 8a). Hence, nano-sized pedogenic hematite is attributed to Comp. 2.

Comp. 3 is easily identified in loess and paleosol because of its high coercivity up to 1.7 T (Fig. 5). Such an exceptionally high coercivity value can only be attributed to antiferromagnetic minerals. Considering Comp. 3 is saturated under ~ 3 T while goethite seldom achieves saturation in such low field (Dekkers, 1989; France and Oldfield, 2000); this excludes goethite. Besides, IRM contributed by Comp. 3 remains relatively constant in dissolution step I but gradually decreases in step II (Fig. 6a and c) while goethite is uniformly removed during dissolution (Fig. 2a). Therefore, hematite is the only candidate in this case. High coercivity (~ 500 – 1800 mT) hematite was also identified in Chinese loess (Eyre, 1996; Kruijer et al., 2001; Spassov et al., 2003; van Oorschot et al., 2002). Such high coercivity especially for SD hematite originates from magnetoelastic anisotropy due to internal stress (Dunlop and Özdemir, 1997) and is strongly dependent on its grain size (Dunlop, 1971). The coercivity of hematite reaches the maximum at the boundary of SD/PSD, which corresponds to tens–hundreds micrometers. In this case, we assign detrital micro-sized hematite as the main carrier of Comp. 3. Once again, the dissolution behavior strongly supports the coarse grain size of Comp. 3 because it was not significantly removed at the initial stage of dissolution (Fig. 6a and c), consistent with the hematite dissolution curves (Fig. 2b).

DRS band analyses also reveal two kinds of hematite. Kosmas et al. (1986) found that the position of characteristic electron pair transition band of hematite at ~ 545 nm (P_{560}), which is characterized by a minimum in the second derivative spectrum of the K–M remission function, was negatively correlated with the degree of Al substitution. Liu et al. (2011) made similar conclusion in Chinese loess/paleosol. Al substitution is omnipresent during weathering process such as those undergone in paleosol development (Cornell and Schwertmann, 2003). Fig. 7a shows that P_{560} continuously increases during the dissolution process of loess samples, indicating that hard-dissolved hematite is more stoichiometric (Liu et al., 2011). In paleosols, the strength of pedogenesis as well as Al-substitution of hematite are significantly enhanced and, because pedogenic hematite dominates the whole population of hematite, the P_{560} value remains consistently low until the final stage of dissolution (Fig. 7b).

In summary, our comprehensive study reveals two kinds of hematite: (1) pedogenic hematite which is nano-sized, magnetically soft, highly Al substituted and less resistant to dissolution; and (2) detrital hematite, which is micro-sized, magnetically hard, more stoichiometric and more resistant to dissolution.

4.2. Quantification of pedogenic components and implications on the mechanism of pedogenic pathway

Quantification of pedogenic hematite is crucial to understand the soil forming processes and their linkage to climate. So far, many approaches were used to quantify the concentration of hematite, such as DRS, X-ray diffraction, Mössbauer spectroscopy (Cornell and Schwertmann, 2003, and references therein). However, these methods mostly focus on the total concentration of

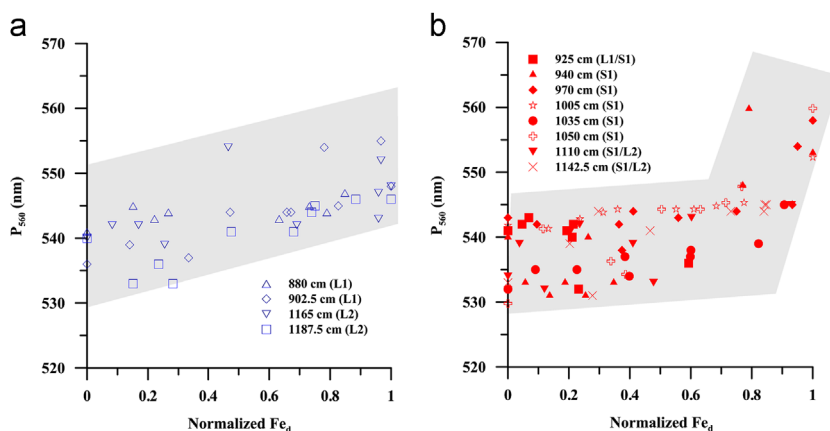


Fig. 7. The change of hematite (P_{560}) characteristic band of loess (a) and paleosol (b) samples during dissolution. Shade areas indicate the changing trend of data during dissolution.

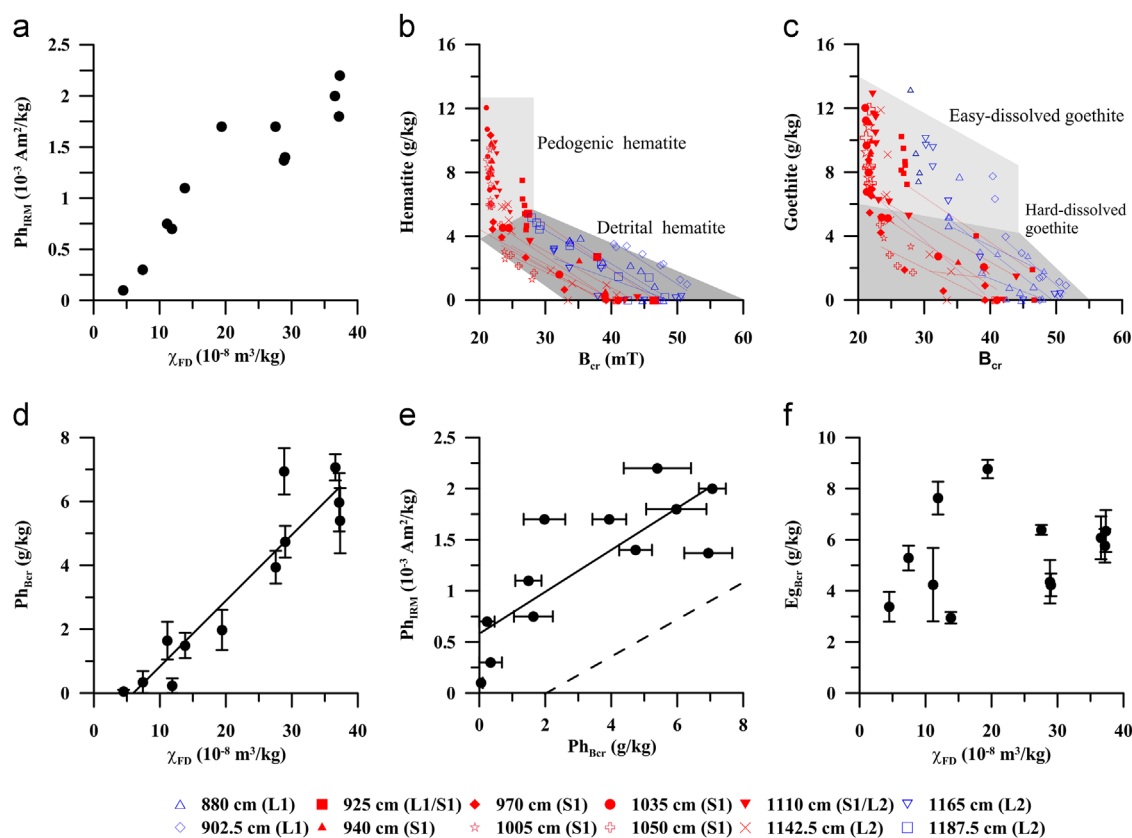


Fig. 8. Quantification of pedogenic hematite: (a) remanent magnetization indicator of pedogenic hematite Ph_{IRM} against χ_{FD} ; (b) relationship between bulk B_{cr} and concentration of hematite, light and dark shade area indicates the dissolution of pedogenic hematite and detrital hematite, respectively; (c) relationship between bulk B_{cr} and concentration of goethite, light and dark shade area indicates the dissolution of easily-dissolved and hard-dissolved goethite, respectively; (d) concentration indicator of pedogenic hematite Ph_{Ber} against χ_{FD} ; (e) relationship between Ph_{IRM} and Ph_{Ber} , dashed line represents the case when SP hematite are largely produced initially (see details in the text); (f) relationship between easily-dissolved goethite (Eg_{Ber}) and χ_{FD} . Error bars for (d), (e) and (f) represent the fitting error in calculating Ph_{Ber} and Eg_{Ber} .

hematite, regardless of its origin. Recently, [Torrent et al. \(2007\)](#) estimated the concentration of pedogenic hematite by subtracting the detrital background while [Hao et al. \(2009\)](#) used the hematite concentration in the clay fraction to represent pedogenic hematite. In this paper, dynamic dissolution and multiple methods enable us to quantify pedogenic hematite on the basis of its own distinct properties.

Firstly, as discussed above, IRM intensity of Comp. 2 can be used as one quantitative indicator (Ph_{IRM}) for pedogenic hematite. For verification, Ph_{IRM} was plotted against χ_{FD} for 12 selected samples. In [Fig. 8a](#), two proxies display excellent positive linear

relationship with χ_{FD} , confirming the pedogenic nature of hematite represented by Ph_{IRM} . However, Ph_{IRM} is a remanent magnetization indicator and therefore cannot reflect hematite below the SP/SD threshold.

In [Fig. 8b](#), pedogenic hematite is quantified by its preferential dissolution nature. Two trends are clearly identified when B_{cr} is plotted against total hematite concentration. In the CLP loess/paleosol samples, B_{cr} is dominated by low coercivity ferrimagnetic minerals ([Evans and Heller, 2001](#)), it hardly changes until magnetite and maghemite start to dissolve. In the initial stage of dissolution, pedogenic hematite significantly dissolves but little

loss of magnetite and maghemite is observed (Figs. 2b–d, 5 and 6a and c). Therefore, B_{cr} remained relatively constant in the first dissolution phase (light grey shaded area in Fig. 8b). Then, in the second phase, B_{cr} gradually increased as pedogenic maghemite (dark grey shaded area) was removed leaving high coercivity particles (Fig. 5). The slope of the corresponding fitting lines is consistent with this observation because lithogenic hematite follows a dissolution trend similar to that of ferrimagnetic minerals (Fig. 2b–d). Therefore, the first phase mainly represents the preferential dissolution of pedogenic hematite. Based on this, we took the hematite concentration at the intersection point of the trends corresponding to the two gray areas as the content of lithogenic hematite. The first trend can be represented by a fitting line parallel to the Y-axis that crosses the X-axis at the average value of B_{cr} in the shaded area. The second trend can be represented by a line calculated via the least square method. The intersection is defined as the cross point of these two fitting lines. Finally, pedogenic hematite content was quantified by subtracting lithogenic hematite from total hematite content, defined as Ph_{Bcr} . Unlike Ph_{IRM} , Ph_{Bcr} is a concentration proxy, including pedogenic hematite of all grain sizes.

As expected, Ph_{Bcr} also displays positive linear relationship with χ_{FD} (Fig. 8d), indicating that the production of pedogenic hematite is closely related to the formation of pedogenic ferrimagnetic minerals. Furthermore, the positive intercept on the χ_{FD} axis gives indirect evidence that pedogenic hematite was mostly formed after pedogenic maghemite at the SP/SD boundary.

To investigate the initial domain state of pedogenic hematite, two quantitative proxies were plotted in the same diagram (Fig. 8e). The fitting trend which illustrates the relationship between mass concentration and remanent magnetism has a positive intercept on the Ph_{IRM} axis, which indicates that pedogenic hematite is produced initially in SD region. If SP particles were produced initially in significant amount, there would be no contribution to IRM but significant mass contribution (i.e. Ph_{IRM} would be close to zero but Ph_{Bcr} would be significantly higher than zero). In that case, the increase in the concentration of pedogenic hematite precedes the increase in remanent magnetism (illustrated by the dash line in Fig. 8e). This result further is consistent with the ferrihydrite → maghemite-like phase → hematite formation model, not only because pedogenic hematite is formed after maghemite during this transformation, but also because the intermediate maghemite grows in size before its transformation into hematite, resulting in SD particles (Liu et al., 2008a; Michel et al., 2010).

Pedogenic SP hematite particles are not significant according to our results although they are observed by Chen et al. (2010). This indicates that other mechanisms could account for the formation of SP hematite during the pedogenesis but are definitely not the dominant mechanism. For example, hematite can be formed directly through ferrihydrite transformation by dehydration and internal rearrangement (Barrón and Torrent, 2002; Cornell and Schwertmann, 2003). But this mechanism can be blocked by adsorbing ligands such as phosphate, which are known to promote the transformation of ferrihydrite into a “hydromaghemite” phase which is later transformed to hematite (Barrón and Torrent, 2002; Barrón et al., 2003; Michel et al., 2010; Torrent et al., 2010). In this study, the Chinese paleosol is a highly weathered and old soil with less doping ligands. Therefore, SP hematite is probably formed via dehydration and rearrangement of the initial ferrihydrite forming from the weathering of Fe-bearing minerals such as clay minerals (Torrent et al., 2007). Due to its extremely small size and little contribution to mass, the DRS and remanence-related proxies cannot sensitively detect them.

For goethite, following the same method, easily-dissolved goethite (Eg_{Bcr}) was also quantified on the Goethite– B_{cr} plot (Fig. 8c). Unlike pedogenic hematite, the easily-dissolved goethite is

widespread in all samples. The χ_{FD} and Eg_{Bcr} show no correlation (Fig. 8f). Meanwhile, the goethite concentration is not enhanced in paleosols. Instead, a systematic up–down increase was found (Fig. 1), which indicates that the goethite concentration reflects the eolian inputs rather than pedogenesis (Chen et al., 2010; Torrent et al., 2007).

4.3. Dissolution behavior of magnetic iron oxides: indication on paleoenvironment

Dissolution of magnetic minerals commonly occurs in lacustrine, marine and even loess/paleosols during temporary water-logging caused by abundant rainfall or groundwater fluctuations (Hu et al., 2009; Liu et al., 2008b; Yin and Guo, 2006). The magnetic granulometric parameters suggest a preferential depletion of finer magnetite grains (Channell and Hawthorne, 1990; Kawamura et al., 2012) while goethite and hematite are generally considered to be more resistant to dissolution (Oldfield et al., 1992; Robinson et al., 2000). However, due to the complex nature of dissolution, no clear-cut dissolution order was achieved; in fact, the stability of magnetic minerals varies greatly depending on specific circumstances (Abrajvitch and Kodama, 2011; Cornell and Schwertmann, 2003; Torrent et al., 2007). Although CBD dissolution may not reflect natural conditions accurately, our results still provide useful information on the preservation ability of magnetic minerals in reducing environment.

In this study, nano-sized pedogenic hematite was dissolved in preference to the most common magnetic iron oxides (Figs. 2b, 5 and 6c). A reasonable explanation could be its smaller size (higher specific surface), which makes it more easily involved in chemical dissolution. TEM studies also demonstrated that pedogenic hematite is in nano-sized ranges with low crystallinity (Chen et al., 2010). Moreover, fine hematite particles often appeared on the edge and surface of ferrimagnetic minerals, where they are more exposed to chemical alternation.

DRS data has shown that pedogenic hematite is less stoichiometric due to high Al substitution (Fig. 7). According to a recent study by Jiang et al. (2012), other factors being similar, grain size of SD Al-hematite gradually decreases with increasing Al substitution and the coercivity force increased firstly and then decreased as Al content ranges from 0 to 27 mol%. This indicates that Al substitution indirectly influences dissolution through particle-size and crystallinity. In contrast, coarse grained detrital hematite is more resistant to dissolution (Figs. 2b, 5 and 6c).

Magnetite/Maghemite also shows a clear grain-sized related dissolution behavior according to Day plots, IRM analyses and low temperature χ_{FD} – T curves (Figs. 3–5), following a dissolution order of SP → SD → PSD. To be specific, both χ_{FD} -carrying SP/SD and finer SP maghemite grains are mainly depleted at Step II, lagging behind the dissolution of pedogenic hematite, indicates the average grain size of χ_{FD} -carrying SP/SD and finer SP maghemite may be larger than nano-sized hematite. But PSD/MD detrital magnetite (Liu et al., 2003; Xie et al., 2009) show strong resistance towards dissolution (Figs. 2c, 5 and 6), which is also consistent with other CBD studies (Fine et al., 1995; Deng et al., 2005).

Among these minerals, goethite exhibits indistinguishable dissolution behavior between loess and paleosols, but two kinds of goethite are still distinguished. The easily-dissolved goethite was more readily dissolved than detrital hematite and ferrimagnetic minerals while hard-dissolved goethite co-varies with detrital hematite. For nano-sized crystals, high surface area greatly increase solubility because surface free energy rather than the properties of the bulk solid, govern the dissolution behavior of iron oxides (Cornell and Schwertmann, 2003).

In all, grain size was the dominant factor influencing dissolution behavior of magnetic iron oxides in Chinese loess. Two

possible applications are also revealed in paleomagnetism and paleoenvironment studies. On the one hand, because pedogenic hematite is firstly destroyed in waterlogging event, the correlation plot of Ph_{BCr} and χ_{FD} can be useful in detecting whether dissolution occurs. Although paleorainfall reconstruction with χ has established a threshold of 1000–1200 mm when reductive dissolution may happen (Balsam et al., 2011 and references therein), Ph_{BCr} appears to be a more sensitive index in well developed soils. This index is similar to the $\Delta Hm/\chi_{FD}$ ratio suggested by Torrent et al. (2007), but unaffected by the variation of detrital input. On the other hand, dynamic CBD dissolution method has proven to be effective in removing both pedogenic hematite and maghemite, with precedence of the former. There is increasing awareness that chemical remanent magnetization is usually carried by pedogenic hematite (Deng et al., 2007; Liu et al., 2010a). CBD extraction can thus be investigated as a more reliable method of chemical demagnetization because it is both effective and controllable. Nevertheless, all these potential applications need to be further explored.

5. Conclusions

Our study successfully discriminated magnetic iron oxides of different origins in Chinese loess/paleosols by integrating chemically dissolution, DRS and rock magnetism methods.

Pedogenic hematite differs from its detrital counterpart in several ways. Magnetically, pedogenic hematite ($B_{1/2}$: ~ 130 mT; DP: 0.1–0.2) has much lower coercivity and narrower distribution than detrital hematite ($B_{1/2}$: ~ 1 T; DP: ~ 0.3). Chemically, pedogenic hematite is preferentially dissolved among iron oxides. Spectroscopically, pedogenic hematite is less stoichiometric than detrital ones.

Pedogenic hematite is quantified both in magnetism and concentration. Its remanent indicator Ph_{IRM} linearly correlates with concentration indicator Ph_{BCr} and further displays a pattern indicating single domain hematite is initially produced. This conclusion provides new constraints on the pedogenic pathway that ferrihydrite can be further evolved into maghemite with grain growing from SP to SD size before its transformation into hematite.

Goethite in loess and paleosol samples is clearly identified by its extremely high coercivity (4–7 T) at low temperature and its uniform dissolution behavior. However, the concentration of goethite is more likely dominated by source input rather than in situ pedogenesis.

All magnetic iron oxides investigated in this study exhibit a strong grain size-dependent dissolution behavior, generally following the order of SP \rightarrow SD \rightarrow PSD.

Acknowledgments

We greatly appreciate two anonymous reviewers and Gideon Henderson (the editor) for constructive comments and language improvements. We also thank Maria Angeles and Mercedes Castro for laboratory assistance. This work was supported by the “Strategic Priority Research Program” of the Chinese Academy of Sciences (XDB03020102) and the National Basic Research Program of China (2013CB956403), and the National Natural Science Foundation of China (Grants 41025013, 40974036, 40821091, 41004023 and 41272202). Q.S. Liu was supported by the ‘100 Talent Program of the Chinese Academy of Sciences’. The contribution of J. Torrent and V. Barrón was partly supported by Spain's Ministerio de Educación y Ciencia, Project AGL2010-15067, and FEDER funds.

References

- Abrajevitch, A., Kodama, K., 2011. Diagenetic sensitivity of paleoenvironmental proxies: a rock magnetic study of Australian continental margin sediments. *Geochim. Geophys. Geosyst.* 12, Q05Z24. <http://dx.doi.org/10.1029/2010gc003481>.
- Balsam, W.L., Ellwood, B.B., Ji, J.F., Williams, E.R., Long, X.Y., El Hassani, A., 2011. Magnetic susceptibility as a proxy for rainfall: worldwide data from tropical and temperate climate. *Quat. Sci. Rev.* 30, 2732–2744.
- Banerjee, S., 1970. Origin of thermoremanence in goethite. *Earth Planet. Sci. Lett.* 8, 197–201.
- Banerjee, S.K., 1971. New grain size limits for palaeomagnetic stability in haematite. *Nat. Phys. Sci.* 232, 15–16.
- Banerjee, S.K., King, J., Marvin, J., 1981. A rapid method for magnetic granulometry with applications to environmental studies. *Geophys. Res. Lett.* 8, 333–336.
- Barrón, V., Torrent, J., 2002. Evidence for a simple pathway to maghemite in Earth and Mars soils. *Geochim. Cosmochim. Acta* 66, 2801–2806.
- Barrón, V., Torrent, J., de Grave, E., 2003. Hydromaghemite, an intermediate in the hydrothermal transformation of 2-line ferrihydrite into hematite. *Am. Mineral.* 88, 1679–1688.
- Barrón, V., Torrent, J., Michel, F.M., 2012. Critical evaluation of the revised akdalaite model for ferrihydrite—Discussion. *Am. Mineral.* 97, 253–254.
- Bloemendal, J., Liu, X.M., Rolph, T.C., 1995. Correlation of the magnetic susceptibility stratigraphy of Chinese loess and the marine oxygen isotope record: chronological and paleoclimatic implications. *Earth Planet. Sci. Lett.* 131, 371–380.
- Bógalo, M.F., Heller, F., Osete, M.L., 2001. Isothermal remanence experiments at room and at liquid nitrogen temperature: application to soil studies. *Geophys. Res. Lett.* 28, 419–422.
- Boyle, J.F., Dearing, J.A., Blundell, A., Hannam, J.A., 2010. Testing competing hypotheses for soil magnetic susceptibility using a new chemical kinetic model. *Geology* 38, 1059–1062.
- Cabello, E., Morales, M.P., Serna, C.J., Barrón, V., Torrent, J., 2009. Magnetic enhancement during the crystallization of ferrihydrite at 25 and 50 °C. *Clays Clay Miner.* 57, 46–53.
- Channell, J.E.T., Hawthorne, T., 1990. Progressive dissolution of titanomagnetites at ODP Site 653 (Tyrrhenian Sea). *Earth Planet. Sci. Lett.* 96, 469–480.
- Chen, J., Ji, J.F., Balsam, W., Chen, Y., Liu, L.W., An, Z.S., 2002. Characterization of the Chinese loess–paleosol stratigraphy by whiteness measurement. *Palaeogeogr. Palaeoclimatol. Palaeoecol.* 183, 287–297.
- Chen, T.H., Xie, Q.Q., Xu, H.F., Chen, J., Ji, J.F., Lu, H.Y., Balsam, W., 2010. Characteristics and formation mechanism of pedogenic hematite in Quaternary Chinese loess and paleosols. *Catena* 81, 217–225.
- Chen, T.H., Xu, H.F., Xie, Q.Q., Chen, J., Ji, J.F., Lu, H.Y., 2005. Characteristics and genesis of maghemite in Chinese loess and paleosols: mechanism for magnetic susceptibility enhancement in paleosols. *Earth Planet. Sci. Lett.* 240, 790–802.
- Cornell, R.M., Schwertmann, U., 2003. *The Iron Oxides: Structure, Properties, Reactions, Occurrences and Uses*. Wiley-VCH, Weinheim, Germany.
- Day, R., Fuller, M., Schmidt, V.A., 1977. Hysteresis properties of titanomagnetites—grain-size and compositional dependence. *Phys. Earth Planet. Inter.* 13, 260–267.
- Dearing, J.A., Hay, K.L., Baban, S.M.J., Huddleston, A.S., Wellington, E.M.H., Loveland, P.J., 1996. Magnetic susceptibility of soil: an evaluation of conflicting theories using a national data set. *Geophys. J. Int.* 127, 728–734.
- Deaton, B.C., Balsam, W.L., 1991. Visible spectroscopy: a rapid method for determining hematite and goethite concentration in geological materials. *J. Sediment. Petrol.* 61, 628–632.
- Dekkers, M.J., 1989. Magnetic properties of natural goethite-I. Grain-size dependence of some low- and high-field related rockmagnetic parameters measured at room temperature. *Geophys. J. Int.* 97, 323–340.
- Dekkers, M.J., Linssen, J.H., 1989. Rockmagnetic properties of fine-grained natural low-temperature hematite with reference to remanence acquisition mechanisms in red beds. *Geophys. J. Int.* 99, 1–18.
- Deng, C., Liu, Q., Wang, W., Liu, C., 2007. Chemical overprint on the natural remanent magnetization of a subtropical red soil sequence in the Bose Basin, southern China. *Geophys. Res. Lett.* 34, L22308. <http://dx.doi.org/10.1029/2007gl031400>.
- Deng, C., Vidic, N.J., Verosub, K.L., Singer, M.J., Liu, Q., Shaw, J., Zhu, R., 2005. Mineral magnetic variation of the Jiaodao Chinese loess/paleosol sequence and its bearing on long-term climatic variability. *J. Geophys. Res.* 110, B03103. <http://dx.doi.org/10.1029/2004jb003451>.
- Dunlop, D.J., 1971. Magnetic properties of fine-particle hematite. *Ann. Geophys.* 27, 269–293.
- Dunlop, D.J., 2002a. Theory and application of the day plot (M_{rs}/M_s versus H_{cr}/H_c) 1. Theoretical curves and tests using titanomagnetite data. *J. Geophys. Res.* 107 (B3), 2056. <http://dx.doi.org/10.1029/2001jb000486>.
- Dunlop, D.J., 2002b. Theory and application of the day plot (M_{rs}/M_s versus H_{cr}/H_c) 2. Application to data for rocks, sediments, and soils. *J. Geophys. Res.* 107 (B3), 2057. <http://dx.doi.org/10.1029/2001jb000487>.
- Dunlop, D.J., Özdemir, Ö., 1997. *Rock Magnetism: Fundamentals and Frontiers*. Cambridge University Press, Cambridge, UK.
- Egli, R., 2004. Characterization of individual rock magnetic components by analysis of remanence curves, 1. Unmixing natural sediments. *Stud. Geophys. Geod.* 48, 391–446.
- Evans, M.E., Heller, F., 1994. Magnetic enhancement and palaeoclimate: study of a loess/paleosol couplet across the loess plateau of China. *Geophys. J. Int.* 117, 257–264.

- Evans, M.E., Heller, F., 2001. Magnetism of loess/palaeosol sequences: recent developments. *Earth Sci. Rev.* 54, 129–144.
- Eyre, J.K., 1996. The application of high resolution IRM acquisition to the discrimination of remanence carriers in Chinese loess. *Stud. Geophys. Geod.* 40, 234–242.
- Fassbinder, J.W.E., Stanjek, H., Vali, H., 1990. Occurrence of magnetic bacteria in soil. *Nature* 343, 161–163.
- Fine, P., Singer, M.J., Verosub, K.L., Tenpas, J., 1993. New evidence for the origin of ferrimagnetic minerals in loess from China. *Soil Sci. Soc. Am. J.* 57, 1537–1542.
- Fine, P., Verosub, K.L., Singer, M.J., 1995. Pedogenic and lithogenic contributions to the magnetic susceptibility record of the Chinese loess/paleosol sequence. *Geophys. J. Int.* 122, 97–107.
- France, D.E., Oldfield, F., 2000. Identifying goethite and hematite from rock magnetic measurements of soils and sediments. *J. Geophys. Res.* 105, 2781–2795, <http://dx.doi.org/10.1029/1999jb000304>.
- Fukuma, K., Torii, M., 1998. Variable shape of magnetic hysteresis loops in the Chinese loess-paleosol sequence. *Earth Planets Space* 50, 9–14.
- Geiss, C.E., Zanner, C.W., 2006. How abundant is pedogenic magnetite? Abundance and grain size estimates for loessic soils based on rock magnetic analyses. *J. Geophys. Res.* 111, B12S21, <http://dx.doi.org/10.1029/2006jb004564>.
- Hao, Q.Z., Oldfield, F., Bloemendal, J., Guo, Z.T., 2008. Particle size separation and evidence for pedogenesis in samples from the Chinese Loess Plateau spanning the past 22 M.Y. *Geology* 36, 727–730.
- Hao, Q., Oldfield, F., Bloemendal, J., Torrent, J., Guo, Z., 2009. The record of changing hematite and goethite accumulation over the past 22 Myr on the Chinese loess plateau from magnetic measurements and diffuse reflectance spectroscopy. *J. Geophys. Res.* 114, B12101, <http://dx.doi.org/10.1029/2009jb006604>.
- Heller, F., Liu, T.S., 1986. Paleoclimatic and sedimentary history from magnetic susceptibility of loess in China. *Geophys. Res. Lett.* 13, 1169–1172.
- Heslop, D., Dekkers, M.J., Kruiver, P.P., van Oorschot, I.H.M., 2002. Analysis of isothermal remanent magnetization acquisition curves using the expectation-maximization algorithm. *Geophys. J. Int.* 148, 58–64.
- Hrouda, F., 2011. Models of frequency-dependent susceptibility of rocks and soils revisited and broadened. *Geophys. J. Int.* 187, 1259–1269.
- Hu, X.F., Wei, J., Xu, L.F., Zhang, G.L., Zhang, W.G., 2009. Magnetic susceptibility of the Quaternary Red Clay in subtropical China and its paleoenvironmental implications. *Palaeogeogr. Palaeoclimatol. Palaeoecol.* 279, 216–232.
- Hunt, C.P., Singer, M.J., Kletetschka, G., Tenpas, J., Verosub, K.L., 1995. Effect of citrate–bicarbonate–dithionite treatment on fine-grained magnetite and maghemite. *Earth Planet. Sci. Lett.* 130, 87–94.
- Ji, J.F., Balsam, W., Chen, J., Liu, L.W., 2002. Rapid and quantitative measurement of hematite and goethite in the Chinese loess–paleosol sequence by diffuse reflectance spectroscopy. *Clays Clay Miner.* 50, 208–216.
- Jiang, Z., Liu, Q., Barrón, V., Torrent, J., Yu, Y., 2012. Magnetic discrimination between Al-substituted hematites synthesized by hydrothermal and thermal dehydration methods and its geological significance. *J. Geophys. Res.* 117, B02102, <http://dx.doi.org/10.1029/2011jb008605>.
- Kawamura, N., Ishikawa, N., Torii, M., 2012. Diagenetic alteration of magnetic minerals in Labrador Sea sediments (IODP sites U1305, U1306, and U1307). *Geochim. Geophys. Res.* 13, Q08013, <http://dx.doi.org/10.1029/2012gc004213>.
- King, J., Banerjee, S.K., Marvin, J., Ozdemir, O., 1982. A comparison of different magnetic methods for determining the relative grain size of magnetite in natural materials: some results from lake sediments. *Earth Planet. Sci. Lett.* 59, 404–419.
- Kletetschka, G., Wasilewski, P.J., 2002. Grain size limit for SD hematite. *Phys. Earth Planet. Inter.* 129, 173–179.
- Kosmas, C.S., Franzmeier, D.P., Schulze, D.G., 1986. Relationship among derivative spectroscopy, color, crystallite dimensions, and Al substitution of synthetic goethites and hematites. *Clays Clay Miner.* 34, 625–634.
- Kruiver, P.P., Dekkers, M.J., Heslop, D., 2001. Quantification of magnetic coercivity components by the analysis of acquisition curves of isothermal remanent magnetisation. *Earth Planet. Sci. Lett.* 189, 269–276.
- Kukla, G., Heller, F., Ming, L.X., Chun, X.T., Sheng, L.T., Sheng, A.Z., 1988. Pleistocene climates in China dated by magnetic susceptibility. *Geology* 16, 811–814.
- Le Borgne, E., 1955. Susceptibilité magnétique anormale du sol superficiel. *Ann. Geophys.* 11, 399–419.
- Liu, C.C., Deng, C.L., Liu, Q.S., Zheng, L.T., Wang, W., Xu, X.M., Huang, S., Yuan, B.Y., 2010a. Mineral magnetism to probe into the nature of palaeomagnetic signals of subtropical red soil sequences in southern China. *Geophys. J. Int.* 181, 1395–1410.
- Liu, Q., Banerjee, S.K., Jackson, M.J., Chen, F., Pan, Y., Zhu, R., 2003. An integrated study of the grain-size-dependent magnetic mineralogy of the Chinese loess/paleosol and its environmental significance. *J. Geophys. Res.* 108, 2437, <http://dx.doi.org/10.1029/2002jb002264>, B9.
- Liu, Q., Barrón, V., Torrent, J., Eeckhout, S.G., Deng, C., 2008a. Magnetism of intermediate hydromaghemite in the transformation of 2-line ferrihydrite into hematite and its paleoenvironmental implications. *J. Geophys. Res.* 113, B01103, <http://dx.doi.org/10.1029/2007jb005207>.
- Liu, Q., Jackson, M.J., Banerjee, S.K., Maher, B.A., Deng, C., Pan, Y., Zhu, R., 2004a. Mechanism of the magnetic susceptibility enhancements of the Chinese loess. *J. Geophys. Res.* 109, B12107, <http://dx.doi.org/10.1029/2004jb003249>.
- Liu, Q., Jackson, M.J., Yu, Y., Chen, F., Deng, C., Zhu, R., 2004b. Grain size distribution of pedogenic magnetic particles in Chinese loess/paleosols. *Geophys. Res. Lett.* 31, L22603, <http://dx.doi.org/10.1029/2004gl021090>.
- Liu, Q., Torrent, J., Maher, B.A., Yu, Y., Deng, C., Zhu, R., Zhao, X., 2005. Quantifying grain size distribution of pedogenic magnetic particles in Chinese loess and its significance for pedogenesis. *J. Geophys. Res.* 110, B11102, <http://dx.doi.org/10.1029/2005gb003726>.
- Liu, Q., Torrent, J., Yu, Y., Deng, C., 2004c. Mechanism of the parasitic remanence of aluminous goethite [α -(Fe, Al)OOH]. *J. Geophys. Res.* 109, B12106, <http://dx.doi.org/10.1029/2004jb003352>.
- Liu, Q., Yu, Y., Torrent, J., Roberts, A.P., Pan, Y., Zhu, R., 2006. Characteristic low-temperature magnetic properties of aluminous goethite [α -(Fe, Al)OOH] explained. *J. Geophys. Res.* 111, B12S34, <http://dx.doi.org/10.1029/2006jb004560>.
- Liu, Q.S., Deng, C.L., Torrent, J., Zhu, R.X., 2007. Review of recent developments in mineral magnetism of the Chinese loess. *Quat. Sci. Rev.* 26, 368–385.
- Liu, Q.S., Hu, P.X., Torrent, J., Barrón, V., Zhao, X.Y., Jiang, Z.X., Su, Y.L., 2010b. Environmental magnetic study of a Xeralf chronosequence in northwestern Spain: indications for pedogenesis. *Palaeogeogr. Palaeoclimatol. Palaeoecol.* 293, 144–156.
- Liu, Q.S., Torrent, J., Barrón, V., Duan, Z.Q., Bloemendal, J., 2011. Quantification of hematite from the visible diffuse reflectance spectrum: effects of aluminium substitution and grain morphology. *Clay Miner.* 46, 137–147.
- Liu, X.M., Liu, T.S., Paul, H., Xia, D.S., Jiri, C.C., Wang, G., 2008b. Two pedogenic models for paleoclimatic records of magnetic susceptibility from Chinese and Siberian loess. *Sci. China, Ser. D: Earth Sci.* 51, 284–293.
- Liu, T.S., Ding, Z.L., 1998. Chinese loess and the paleomonsoon. *Annu. Rev. Earth Planet. Sci.* 26, 111–145.
- Lovley, D.R., Stolz, J.F., Nord, G.L., Phillips, E.J.P., 1987. Anaerobic production of magnetite by a dissimilatory iron-reducing microorganism. *Nature* 330, 252–254.
- Maher, B.A., 1988. Magnetic properties of some synthetic sub-micron magnetites. *Geophys. J.* 94, 83–96.
- Maher, B.A., 1998. Magnetic properties of modern soils and quaternary loessic paleosols: paleoclimatic implications. *Palaeogeogr. Palaeoclimatol. Palaeoecol.* 137, 25–54.
- Maher, B.A., Karoukouski, V.V., Mutch, T.J., 2004. High-field remanence properties of synthetic and natural submicrometre haematites and goethites: significance for environmental contexts. *Earth Planet. Sci. Lett.* 226, 491–505.
- Maher, B.A., Taylor, R.M., 1988. Formation of ultrafine-grained magnetite in soils. *Nature* 336, 368–370.
- Mehra, O.P., Jackson, M.J., 1960. Iron oxide removal from soils and clays by a dithionite–citrate system buffered with sodium bicarbonate. *Clays Clay Miner.* 7, 317–327.
- Michel, F.M., Barrón, V., Torrent, J., Morales, M.P., Serna, C.J., Boily, J.F., Liu, Q.S., Ambrosini, A., Cismasu, A.C., Brown, G.E., 2010. Ordered ferrimagnetic form of ferrihydrite reveals links among structure, composition, and magnetism. *Proc. Natl. Acad. Sci. USA* 107, 2787–2792.
- Mullins, C.E., 1977. Magnetic susceptibility of soil and its significance in soil science—a review. *J. Soil Sci.* 28, 223–246.
- Oldfield, F., Darnley, I., Yates, G., France, D.E., Hilton, J., 1992. Storage diagenesis versus sulphide authigenesis: possible implications in environmental magnetism. *J. Paleolimnol.* 7, 179–189.
- Oldfield, F., Hao, Q.Z., Bloemendal, J., Gibbs-Eggar, Z., Patil, S., Guo, Z.T., 2009. Links between bulk sediment particle size and magnetic grain-size: general observations and implications for Chinese loess studies. *Sedimentology* 56, 2091–2106.
- Oldfield, F., Yu, L., 1994. The influence of particle size variations on the magnetic properties of sediments from the north-eastern Irish Sea. *Sedimentology* 41, 1093–1108.
- Olson, R.V., Ellis, R., 1982. Iron. In: methods of soil analysis. In: Page, A.L. (Ed.), Part 2. Chemical and Microbiological Properties. American Society of Agronomy and Soil Science Society of America, Madison, WI, pp. 301–312.
- Özdemir, Ö., Dunlop, D.L., 1996. Thermoremanence and Néel temperature of goethite. *Geophys. Res. Lett.* 23, 921–924.
- Quinton, E.E., Dahms, D.E., Geiss, C.E., 2011. Magnetic analyses of soils from the Wind River Range, Wyoming, constrain rates and pathways of magnetic enhancement for soils from semiarid climates. *Geochim. Geophys. Res.* 12, Q07Z30, <http://dx.doi.org/10.1029/2011gc003728>.
- Rath, C., Sahu, K.K., Kulkarni, S.D., Anand, S., Date, S.K., Das, R.P., Mishra, N.C., 1999. Microstructure-dependent coercivity in monodispersed hematite particles. *Appl. Phys. Lett.* 75, 4171–4173.
- Robertson, D.J., France, D.E., 1994. Discrimination of remanence-carrying minerals in mixtures, using isothermal remanent magnetization acquisition curves. *Phys. Earth Planet. Inter.* 82, 223–234.
- Robinson, S.G., Sahota, J.T.S., Oldfield, F., 2000. Early diagenesis in north atlantic abyssal plain sediments characterized by rock-magnetic and geochemical indices. *Mar. Geol.* 163, 77–107.
- Rochette, P., Mathé, P.-E., Esteban, L., Rakoto, H., Bouchez, J.-L., Liu, Q., Torrent, J., 2005. Non-saturation of the defect moment of goethite and fine-grained hematite up to 57 T. *Geophys. Res. Lett.* 32, L22309, <http://dx.doi.org/10.1029/2005gl024196>.
- Sartori, M., Evans, M.E., Heller, F., Tsatskin, A., Han, J.M., 2005. The last glacial/interglacial cycle at two sites in the Chinese Loess Plateau: mineral magnetic, grain-size and Be¹⁰ measurements and estimates of palaeoprecipitation. *Palaeogeogr. Palaeoclimatol. Palaeoecol.* 222, 145–160.
- Singer, M.J., Bowen, L.H., Verosub, K.L., Fine, P., Tenpas, J., 1995. Mössbauer spectroscopic evidence for citrate–bicarbonate–dithionite extraction of maghemite from soils. *Clays Clay Miner.* 43, 1–7.
- Singer, M.J., Verosub, K.L., Fine, P., Tenpas, J., 1996. A conceptual model for the enhancement of magnetic susceptibility in soils. *Quat. Int.* 34–36, 243–248.
- Spassov, S., Heller, F., Kretschmar, R., Evans, M.E., Yue, L.P., Nourgaliev, D.K., 2003. Detrital and pedogenic magnetic mineral phases in the loess/paleosol

- sequence at Lingtai (central Chinese Loess Plateau). *Phys. Earth Planet. Inter.* 140, 255–275.
- Torrent, J., Barrón, V., 2003. The visible diffuse reflectance spectrum in relation to the color and crystal properties of hematite. *Clays Clay Miner.* 51, 309–317.
- Torrent, J., Barrón, V., Liu, Q., 2006. Magnetic enhancement is linked to and precedes hematite formation in aerobic soil. *Geophys. Res. Lett.* 33, L02401, <http://dx.doi.org/10.1029/2005gl024818>.
- Torrent, J., Liu, Q.S., Barrón, V., 2010. Magnetic susceptibility changes in relation to pedogenesis in a Xeralf chronosequence in northwestern Spain. *Eur. J. Soil Sci.* 61, 161–173.
- Torrent, J., Liu, Q.S., Bloemendal, J., Barrón, V., 2007. Magnetic enhancement and iron oxides in the upper luochuan loess–paleosol sequence, Chinese Loess Plateau. *Soil Sci. Soc. Am. J.* 71, 1570–1578.
- van Oorschot, I.H.M., Dekkers, M.J., Havlicek, P., 2002. Selective dissolution of magnetic iron oxides with the acid-ammonium-oxalate/ferrous-iron extraction technique—II. Natural loess and palaeosol samples. *Geophys. J. Int.* 149, 106–117.
- van Velzen, A.J., Dekkers, M.J., 1999. Low-temperature oxidation of magnetite in loess-paleosol sequences: a correction of rock magnetic parameters. *Stud. Geophys. Geod.* 43, 357–375.
- Verosub, K.L., Roberts, A.P., 1995. Environmental magnetism: past, present, and future. *J. Geophys. Res.* 100, 2175–2192, <http://dx.doi.org/10.1029/94jb02713>.
- Worm, H.U., 1998. On the superparamagnetic-stable single domain transition for magnetite, and frequency dependence of susceptibility. *Geophys. J. Int.* 133, 201–206.
- Xie, Q.Q., Chen, T.H., Xu, X.C., Qing, C.S., Xu, H.F., Sun, Y.B., Ji, J.F., 2009. Transformation relationship among different magnetic minerals within loess-paleosol sediments of the Chinese Loess Plateau. *Sci. China, Ser. D: Earth Sci.* 52, 313–322.
- Xu, X.W., Qiang, X.K., Fu, C.F., Zhao, H., Chen, T., Sun, Y.F., 2012. Characteristics of frequency-dependent magnetic susceptibility in Bartington MS2 and Kappa-bridge MFK1-FA, and its application in loess-paleosol, red clay and lacustrine sediments. *Chin. J. Geophys.* 55, 197–206.
- Yin, Q.Z., Guo, Z.T., 2006. Mid-pleistocene vermiculated red soils in southern china as an indication of unusually strengthened East Asian monsoon. *Chin. Sci. Bull.* 51, 213–220.
- Zheng, H.B., Oldfield, F., Yu, L.H., Shaw, J., An, Z.S., 1991. The magnetic-properties of particle-sized samples from the Luo Chuan Loess Section: evidence for pedogenesis. *Phys. Earth Planet. Inter.* 68, 250–258.
- Zhou, L.P., Oldfield, F., Wintle, A.G., Robinson, S.G., Wang, J.T., 1990. Partly pedogenic origin of magnetic variations in Chinese loess. *Nature* 346, 737–739.